ELSEVIER

Sensors and Actuators 73 (1999) 80–88

SENSORS AND ACTUATORS A PHYSICAL

Sensors and actuators on non-planar substrates

Wen J. Li [a,*], John D. Mai [b], Chih-Ming Ho [b]

[a] *Department of Mechanical and Automation Engineering, The Chinese University of Hong Kong, Room 617, Ho Sin-Hang Eng. Bldg., Shatin, New Territories, Hong Kong, China*

[b] *Department of Mechanical and Aerospace Engineering, University of California at Los Angeles, Room 44-121, Eng. IV Bldg., Los Angeles, CA 90095, USA*

Received 16 April 1998; accepted 7 October 1998

Abstract

The integration of MEMS sensors and actuators onto macro mechanical parts is a critical technology necessary for the potential realization of intelligent mechanical structures. The current planar fabrication methods offered by the MEMS/IC industry restrict the possibility of integrating micro devices onto contoured (non-planar) mechanical structures. We have developed a lithographic technique to directly fabricate micron-sized sensing and actuation devices onto a cylindrical surface. This novel technology encompasses the development of flexible masks, photoresist spraying technique, and customized alignment systems. Results indicate that line resolution of $< 5\ \mu m$ is possible for structures on the surface of a 2″ (5.08 cm) long cylinder with a diameter of 1.25″ (3.175 cm). This paper describes the procedures developed to fabricate sacrificially release micro structures onto a cylindrical surface. The performance of micro thermal actuators and shear stress sensors on a quartz cylindrical substrate are also presented.

Keywords: Non-planar substrate; Contoured substrate; Non-planar lithography; Flexible mask; Cylindrical substrate; Intelligent structures

1. Introduction

Attempts to create mechanical components that can sense and control their environment are underway. Sensing very complex physical phenomena such as turbulent shear stress using MEMS sensors and the control of skin friction by MEMS actuators on a flat plate have already been demonstrated by Ho et al. in 1994 [1]. Currently, the total integration of sensors, actuators, and decision making IC components for flow control are under investigation by CIT/UCLA [2]. Besides aerodynamic flow control and monitoring, other proposed applications for integrated MEMS-mechanical systems are condition-based maintenance, environmental monitoring, process control, robotics, and automation [3,4]. Since standard MEMS/IC process technology only allows the fabrication of microstructures on flat substrates, the MEMS/IC components must reside on a flat chip. Typically, the micromachined devices are implanted onto mechanical surfaces that are pre-machined with recesses to accommodate the devices [1]. Other methods include fitting hermetically sealed sensor and circuit system into machined parts [3]. Thus, the packaging of chips onto macro mechanical parts often changes the contour of the macro substrates, which, in some cases, can be detrimental to the function of the macro components. For instance, changing the leading edge contour of an airfoil can significantly decrease lift on the airfoil.

Methods such as epitaxial lift-off [5] and total-substrate-removal [6] were developed to put optical and electronic devices such as diode lasers and HEMTs (high electron mobility transistors) on flexible substrates that can be bonded to arbitrary substrates. Using similar techniques, CIT/UCLA have fabricated surface-micromachined shear stress sensors on flexible substrates that can be conformed to non-planar macro mechanical parts [7]. The flexible-substrate method offers the advantage of producing functional devices using a fully IC compatible process. However, this approach lacks the capability to *bulk-micromachine* contoured mechanical substrates. Also, glue uniformity, stress induced by the glue on the film, and alignment of the films to a desired orientation are some of the issues to be addressed when this approach is used.

Other methods such as direct-write [8], flexible stamp [9], direct-tooling [10], and shadow-masking can also be

* Corresponding author. Tel.: +852-2609-8475; Fax: +852-2603-6002; E-mail: wen@mae.cuhk.edu.hk

0924-4247/99/$ - see front matter
PII: S0924-4247(98)00258-1

used to produce microstructures on a contoured surface. However, to the best of our knowledge, no work has reported a procedure to align multiple masks of images or produced sacrificially released microstructures on a macro non-planar surface.

2. The flexible mask technique

We have developed a technique to directly fabricate sacrificially released micro sensors and actuators onto the surface of a macro cylindrical substrate. The important aspects of this technique are the development of the flexible masks (FM), spray of photoresist onto a contoured substrate, and a method to correct alignment errors.

2.1. Flexible masks

A flexible UV-transparent material can be used as a flexible mask that conforms to non-planar surfaces if non-UV-transparent micron-sized structures can be patterned on it. As illustrated in Fig. 1, non-UV-transparent thin films such as Cr or Au can be evaporated onto a flexible material and then patterned using conventional microlithographic procedures such as spin-on photoresist and contact UV exposure. Hence, the image resolution on the flexible masks has the theoretical limit as conventional IC technology. An E-beam can also be used to directly write patterns onto the flexible masks, making submicron resolution possible.

The major problem encountered during the development of the flexible masks was the cracking in the thin film structures on the masks. Mismatch of the expansion coefficients between the thin film material and the flexible material was determined to be the primary cause of this problem [11]. This issue was resolved by using an appropriately thick flexible material and minimizing the rigid substrate temperature during thin film evaporation. Any commercial UV transparent films which are resistant to Au and Cr etchants can be used as the flexible mask material. The following process is suggested to prepare the flexible masks.

1. *Support-substrate cleaning*
   - A quartz or glass plate can be used as the support-substrate for the flexible masks. It should be thoroughly cleaned using RCA solutions before use.
2. *Flexible material cleaning*
   - The flexible material should be cleaned in the Microclean® solution and then rinsed thoroughly.
3. *Secure flexible material to support-substrate*
   - To minimize the residual stress on the flexible material during metal evaporation, do not fix all sides of the flexible material to the support-substrate.
4. *Evaporation of Cr / Au onto flexible material*
   - Use a water-cooled chuck to hold the support-substrate if possible.
   - Evaporate 500 Å of Cr and 2500 Å of Au
5. *Lithography procedures*
   - Pour before spin.
   - Remove the flexible material from the support-substrate and clean the back of the flexible material with solvent. If this step is ignored, bubbles will form between the flexible material and the support-substrate during prebake, which will permanently damage the flexible material.
   - Standard lithography: prebake on 95°C hot plate for 2′; 45″ UV exposure (312 nm, 220 W/cm^2); develop in 4:1 of DI:AZ400 K developer solution for ~ 30 s; postbake on 125°C hot plate for 15′.
6. *Etch Cr and Au*
   - Au (DI:KI:I^2 of 800 ml:80 g:20 g) for ~ 2′.
   - Cr (commercial) etchant for ~ 30″.
7. *Photoresist cleaning*
   - Strip photoresist using methanol (acetone may attack some commercial flexible materials).
   - O_2 plasma clean for 5′ at 100 W, 0.5 mT.

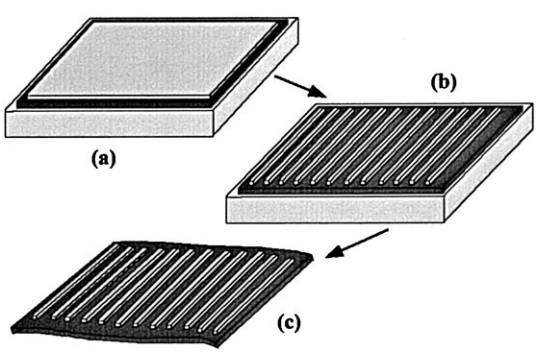

Fig. 1. Procedure for making the flexible masks. (a) Non-UV-transparent thin film can be evaporated onto a flexible material which is then affixed to a rigid substrate before spinning on photoresist. (b) Use conventional lithographic techniques to transfer patterns. (c) The rigid substrate is removed, leaving a patterned flexible mask.

2.2. Photoresist spraying

Spin coating achieves resist uniformity by balancing two forces: the rotation-induced centrifugal force that drives the flow radially outward, and the resisting viscous force that acts radially inward. Therefore, spin coating will not work for coating cylinders due to the imbalance of centrifugal and viscous forces: the centrifugal force acts in the radial direction while the viscous force acts circumferentially and axially on the cylinder surface. Techniques such as spray-coating, dip-coating, slot-coating, taped-resist, evaporated-resist, and electroplated-resist can be used to coat photoresist onto contoured substrates. We have selected spray-coating to coat the cylinder based on cost and resist thickness considerations. From experiments, the important parameters that govern resist uniformity and thick-

ness are the resist droplet size and the distance of the nozzle from the substrate. The droplet size is controlled by the nitrogen gas pressure, the size of the nozzle outlet, and the viscosity of the photoresist. If these parameters are not optimized, defects in the resist will appear across the substrate. Using AZ5206, resist thickness of 0.6 μm with 0.16 μm standard deviation can be obtained across the surface of the cylindrical substrates [11].

2.3. Substrate temperature

For positive photoresist, the prebake, exposure, and development conditions are important in determining resist image edge wall, critical dimension control, and resist sensitivity. The significant parameters are prebake temperature and time, exposure level, and developer composition. All of these variables can potentially interact, therefore, statistical engineering methods and experimental designs are typically used to optimize the overall resist process [12,13]. The prebake stage is strongly affected by the heat transfer conditions, hence, the thermal conductivity and heat capacitance of the substrate material become important. Since quartz cylindrical substrates have different physical dimensions and thermal properties than conventional flat Si substrates, the prebake temperature and duration must be determined experimentally in order to successfully pattern the photoresist on the cylindrical surface. The difference in the temperature history on a flat Si substrate surface and a cylinder substrate surface are shown in Figs. 2 and 3.

Three measurements were made using a thermocouple to obtain the surface temperature at the center of a Si substrate. Measurements showed that, if heated on a 95°C hot plate, the Si surface rises to 80°C within 30 s; it then cools to room temperature within 3 min through natural convection after removal from the hot plate (see Fig. 2). A Comparison was made by heating a representative aluminum cylinder from one of its flat ends while measuring the axially-centered temperature at its surface. For a cylinder (2″ long and diameter of 1.25″) on a 95°C hot plate, ~15 min is required to heat it to 80°C and >35 min is required to cool the cylinder from 80°C to room temperature by natural convection. Conduction cooling by placing the cylinder on top of a cooling plate can reduce this time by >20 min (see Fig. 3). Hence, it is extremely important to calibrate the prebake temperature for non-conventional substrates.

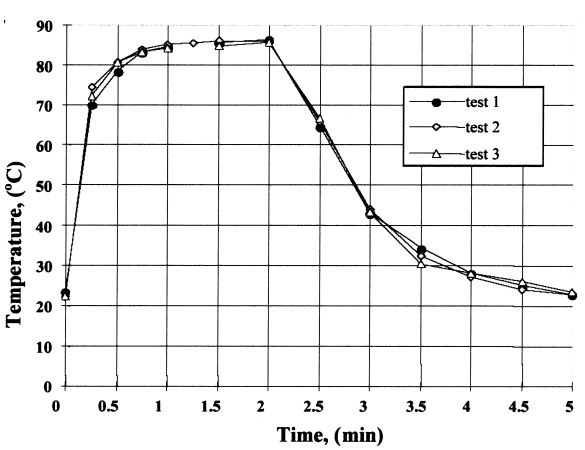

Fig. 2. Temperature profile of flat 3″ Si substrate heated on a 95°C hotplate for 2 min.

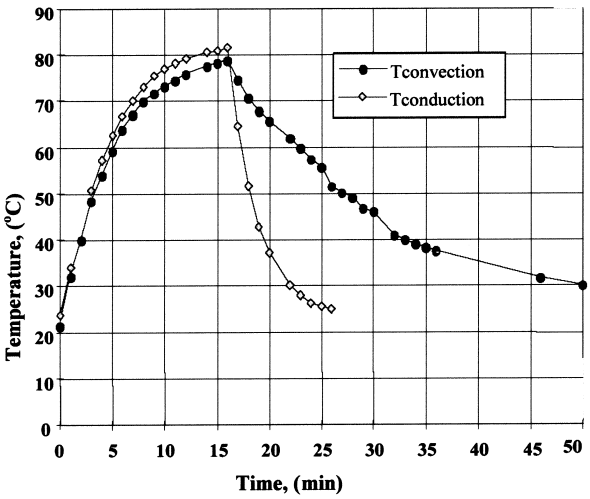

Fig. 3. Conduction and convection cooling effects on the temperature distribution of the surface of a 2″ long 1.5″ diameter Al cylinder.

Using flexible masks, spraying of photoresist, and rotating the substrate during UV exposure, micron-sized struc-

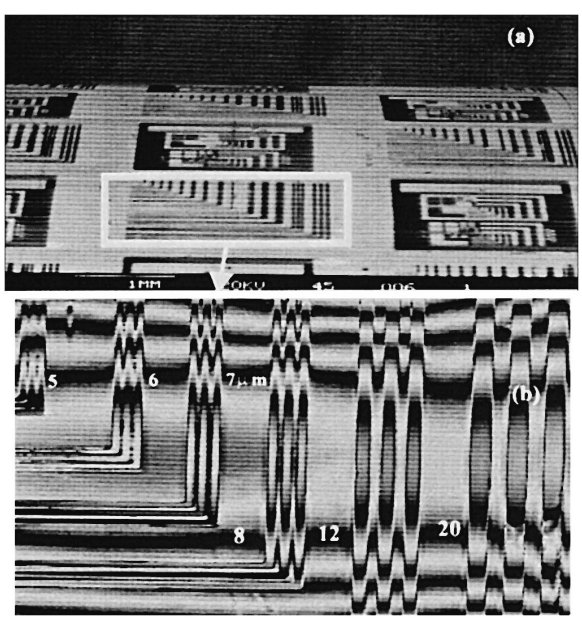

Fig. 4. (a) SEM picture of Au microstructures on a quartz cylindrical substrate surface. (b) Whitelight interferometer image of sample width/gap Au structures on the same substrate. The fringes indicate the substrate curvature.

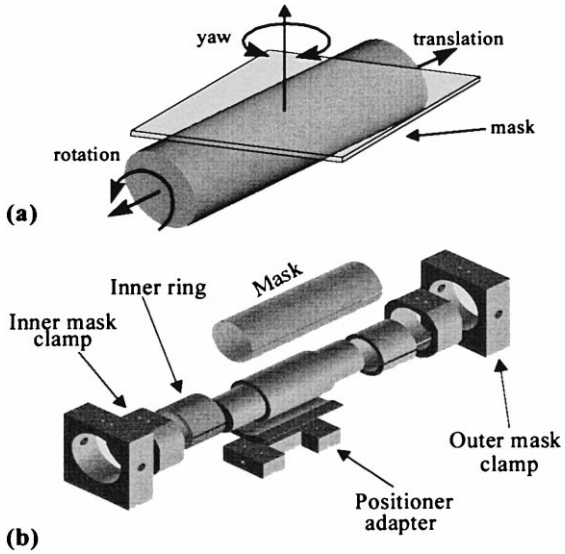

Fig. 5. (a) The 3 possible misalignment errors. (b) Components of the rotation–translation-system.

tures can be directly patterned onto the surface of a non-planar substrate. Micron-sized structures were successfully patterned onto the surface of a 1.25″ diameter, 2″ long cylinder as shown in Fig. 4.

2.4. The customized alignment system

The three possible alignment errors between patterns on a cylindrical surface and on a flexible mask are shown in Fig. 5a. In order to correct these errors, two separate alignment systems were built. A yaw-system was used to adjust the relative yaw error. A rotation–translation-system was used to correct the axial and circumferential errors [11]. During the alignment process, the yaw error is first corrected by the yaw-system. Then, the mask is clamped to the cylinder by a custom-made clamp to fix the yaw position. The mask-cylinder-clamp system is then transferred to the rotation–translation-system for subsequent circumferential and axial error corrections. After the desired alignment is obtained, the mask is made to conformally contact the surface of the cylinder by applying circumferentially distributed radial forces at the ends of the cylinder. An illustration of the rotation–translation system is also shown in Fig. 5b. The inner mask clamps and rings allow the substrate to translate and rotate relative to the mask. Once the positioning errors are corrected, the outer mask clamps apply uniform radial forces on the mask to conform it to the cylindrical substrate. The current alignment resolution is ~ 20 μm due to excessive stretching of the masks when conformal radial forces are applied.

3. Sacrificially released structures

A fabrication process was developed to create sacrificially release structures that were used as thermal actuators, temperature sensors, and shear stress sensors. This dry sacrificial process is briefly described below:

1. Evaporate Cr/Au (300 Å/2500 Å) onto a quartz cylindrical substrate. The substrate is rotated during evaporation.
2. Use the FM technique described in the previous section to pattern interconnects and contact pads.
3. Spray AZ5210 photoresist onto the cylindrical substrate and define via with a 2nd mask. This resist layer is used as the sacrificial material.
4. Evaporate Cr/Au/Ti (300 Å/7000 Å/1000 Å) onto the cylindrical substrate. The structural layers are defined by spraying AZ5206 photoresist, using a 3rd mask, and the customized alignment systems.
5. Sacrificially release the structures by etching the resist layer in an O_2 plasma asher.

The parameters of the process were determined by first fabricating the test structures on flat substrates. The same parameters were then used to fabricate the thermal sensors and actuators on cylindrical substrates. Sample structures on a flat substrate using the above process are shown in Fig. 6.

Micro structures on a quartz cylindrical substrate made using the same process are shown in Figs. 7 and 8. The suspended structures shown in Fig. 7 were used as temperature and shear stress sensors; the structures shown in Fig. 8 were used as thermal actuators. The performance of

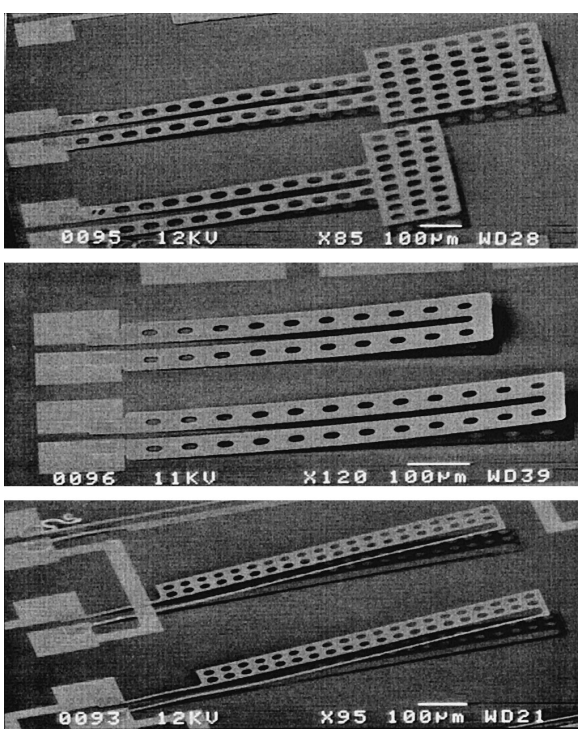

Fig. 6. Sacrificially released structures on a flat Si substrate using the dry-release.

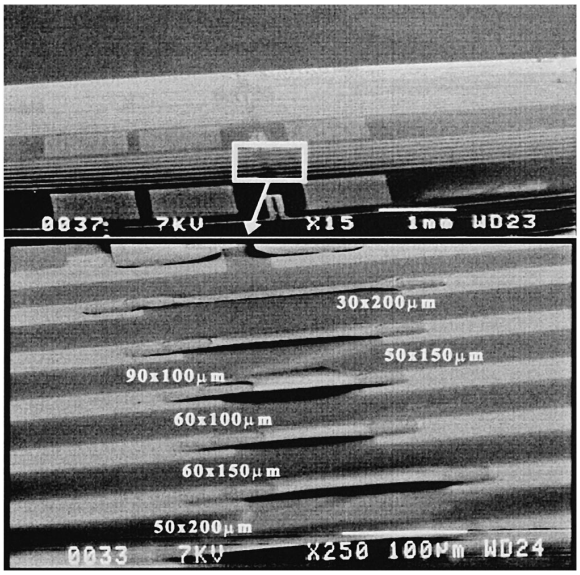

Fig. 7. Sacrificially released Cr/Au/Ti structures on the surface of a quartz cylindrical substrate which were used as thermal actuators.

these sensors and actuators will be presented in the next two sections.

A one-mask process was also developed to sacrificially release micro Cr/Au structures. The patterned Cr/Au structures can be used to mask the bulk quartz substrate in a 49% HF etch bath. After sufficient etch time in the HF, over-etch of the bulk quartz material will release the Cr/Au structures. Samples of the bulk-released structures using this wet-release process are shown in Fig. 9. These

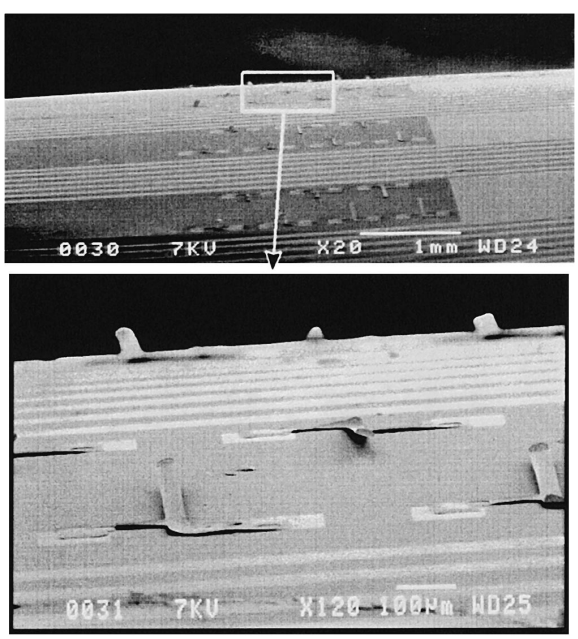

Fig. 8. Sacrificially released Cr/Au/Ti structures on the surface of a quartz cylindrical substrate which were used as thermal actuators.

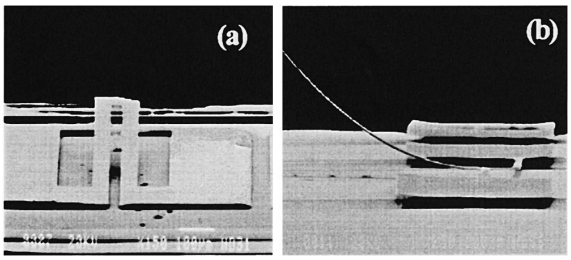

Fig. 9. Sacrificially bulk-released Cr/Au structures on the surface of a quartz cylindrical substrate.

simple structures were also demonstrated as thermal bimorph and lateral actuators.

4. Thermal actuators

The structures shown in Figs. 8 and 9b can be used as lateral thermal actuators. A net lateral motion can be induced at the tip of the long arm by generating thermal strains in the 2 short arms perpendicular to it. As shown in Fig. 10, when the arms with lengths L_1 and L_2 are thermally expanded, the long appendage (length L) will deflect to the right. The tip deflection, δ, of the long appendage can be approximated by geometric considerations. If δ is assumed to be small, it can be represented as a function of the thermal strains ε (assume ε_1 and ε_2 are equal):

$$\delta = L\cos\left[\tan^{-1}(d/2\varepsilon)\right] - \varepsilon \quad (1)$$

The thermal strains can be found by multiplying the thermal expansion coefficient, α, with the rise in temperature of the structures, ΔT. The temperature rise in the structures due to resistive heating can be found by invoking the energy conservation law: the rate of energy generated minus the rate of energy leaving a control volume should be equal to the energy stored in the volume. The heat energy generated depends on the electrical current passing through the structures and the electrical resistance of the structures (I^2R); the energy leaving the control volume is due to conduction to the substrate and free

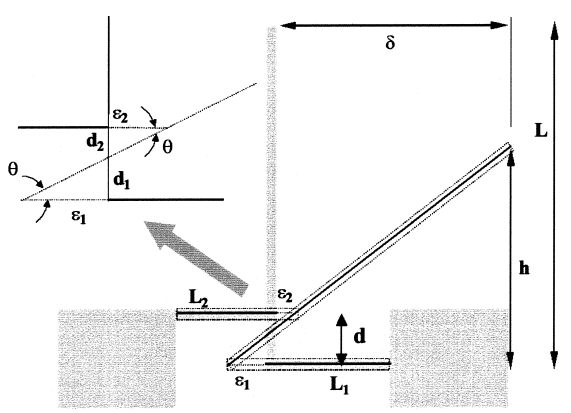

Fig. 10. Geometric parameters of the lateral thermal actuators.

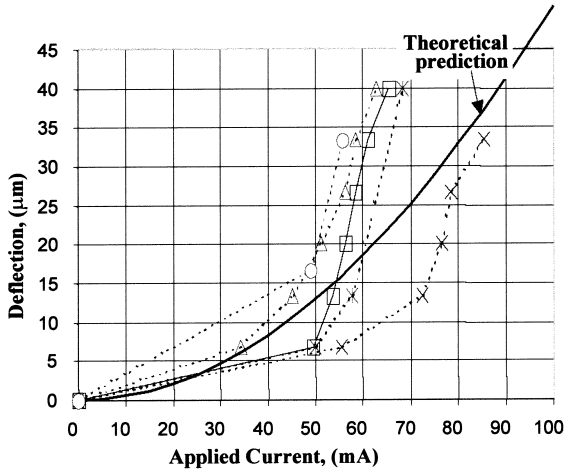

Fig. 11. Theoretical calculations are compared with the experimental results for 5 lateral thermal actuators on a quartz cylindrical substrate.

convection to the surrounding air. The energy stored depends on the volume, density, and specific heat of the structures. The steady-state solution for the energy balance equation is [12]:

$$\Delta T = I^2R/\left[hA_1 + KA_2/x\right] \tag{2}$$

where h and K are the convective and conductive coefficients, respectively; A_1 and A_2 are the corresponding effective areas for conduction and convection, and x is the conduction length. In general, for free convection in air, the conduction term dominates in the above equation if the structural dimensions are in the orders of microns. Then, Eq. (1) can be expressed as:

$$\delta = L\cos\left[\tan^{-1}\left\{d/\left[2\alpha I^2R/(KA_1/x)\right]\right\}\right] - \left[\frac{\alpha I^2R}{KA_1/x}\right] \tag{3}$$

Using the above equation, the theoretical deflections were tabulated and compared to the experimental results as shown in Fig. 11. The dimensions of the lateral actuators were $L = 300$ μm, $L_1 = L_2 = 100$ μm, $d = 100$ μm, and each appendage is 50 μm wide. The resistance of these actuators were measured to be $\sim 1\ \Omega$, which corresponds to using the averaged resistivity for Au and Ti to calculate the resistance. In the calculation of thermal strain caused by I^2R, the thermal conductivity for quartz (11 W/m per °C) was used to determine the conductive heat dissipation. The disagreement between the experimental and theoretical results can be attributed to the crude first-order analysis, i.e., non-temperature dependence of resistivity and small angle approximation of deflections.

5. Thermal sensors

The suspended bridge structures shown in Fig. 7 were tested as two different types of thermal sensors: temperature and shear stress. The resistance of some resistive materials have a strong dependence on temperature and are, therefore, suitable for use as sensors to detect temperature change. Also, when the temperature of a resistor is elevated by Joule heating, the resistive element can be used as a shear stress sensor. The rate of heat loss from the heated element to the airflow is dependent on the velocity profile inside the boundary layer, and hence, the flow shear stress. The relationship between resistance, temperature, and power input are discussed below.

5.1. Temperature sensors

The resistance, R, of a semiconductor or metal resistive element at a given temperature T is [14]:

$$R(T) = R_o\left[1 + \alpha(T - T_o)\right] \tag{4}$$

where R_o is the resistance at room temperature T_o, and β is the temperature coefficient of resistance (TCR). In general, β can also be a function of temperature. Therefore, if T_o, β, and R_o are known, the temperature of the resistor can be determined by measuring the resistance. To determine the TCR of the suspended Cr/Au/Ti elements, the cylinder was packaged as shown in Fig. 12. The suspended elements shown in Fig. 7 are connected to 100 μm metallization lines that terminate at 2 mm × 2 mm bonding pads. Instead of wirebonding, wire-wrapping wires were initially bonded to the edge of the cylinder by commercial 5-min epoxy. The tips of the wires are then bonded to the boding pads by conductive silver epoxy. The other end of the wires can then be connected to the measurement equipment directly.

The packaged cylinder was placed in an isothermal oven for TCR measurement. By varying the temperature and measuring the resulting change in sensor resistance, Fig. 13 was constructed. The TCR of the bridges were found to be $\sim 0.2\%/°C$ as shown in the figure. The averaged known TCR for Cr/Au/Ti is $\sim 0.3\%/°C$, which is comparable to this measured value.

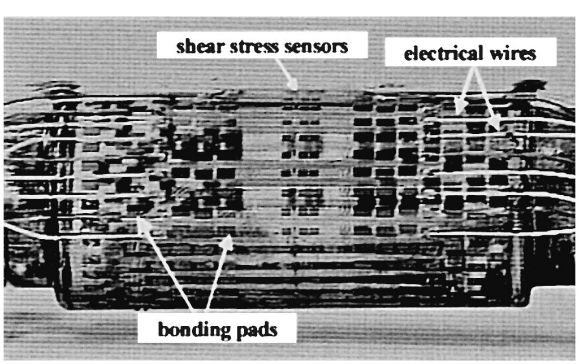

Fig. 12. A packaged quartz cylinder which has micromachined shear stress sensors on the surface.

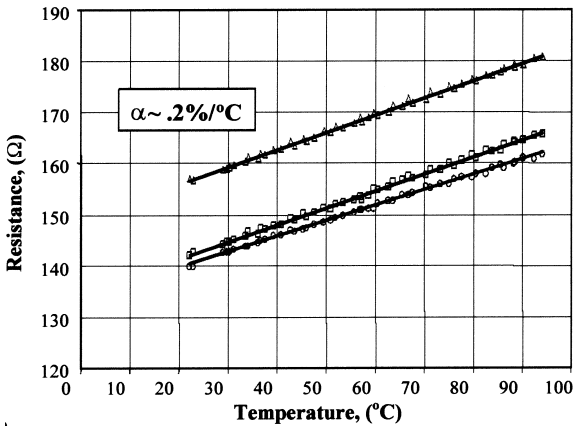

Fig. 13. The measured TCR of the Cr/Au/Ti suspended bridges on the surface of a quartz cylindrical substrate.

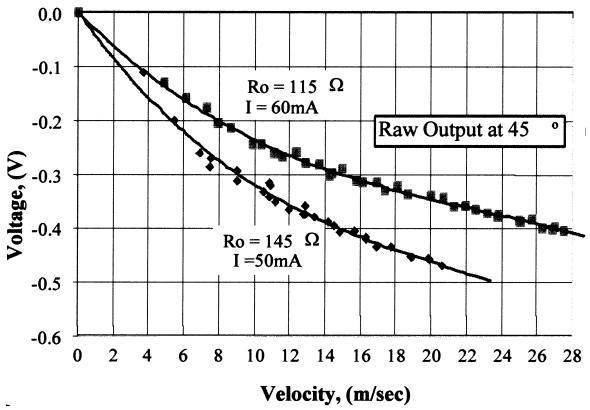

Fig. 15. Raw voltage output of the shear stress sensors on a quartz cylindrical substrate.

5.2. Shear stress sensors

The rate of heat transferred from the resistive element to the flow field depends on the temperature of the resistor and the velocity profile inside the boundary layer. Therefore, by monitoring the change of the electrical characteristics of the heated resistor, flow shear stress on the surface of a body can be transduced into electrical signal. Using the heat energy balance for a shear stress sensor and Fick's Law of diffusion, the power of a heated resistive sensor can be related to the flow shear stress as [12]:

$$I^2R = \Delta T(A\tau^{1/3} + B) \quad (5)$$

where τ is the shear stress, B is the heat loss due to conduction to the substrate, and A is defined as:

$$A = 0.807[CK\rho/L\mu]^{1/3} \quad (6)$$

where C, K, ρ, and μ are the fluid heat capacitance, heat conductance, density, and viscosity, respectively; L is the streamwise length of the heated element. From Eq. (5), if a constant current is provided to heat the sensor, the voltage output of the sensor should be proportional to $1/3$ power of the flow shear stress. Also from Eq. (5), conduction of heat from the sensor to the substrate must be minimized to maximize the sensitivity of the sensor. Hence, suspending the resistive elements off the substrate is a critical requirement for shear stress measurement.

The cylinder shown in Fig. 12 was tested in a windtunnel for shear stress measurement. The cylinder was attached vertically to a rotation platform, as shown in Fig. 14, such that sensors can be oriented at different incident angles from the freestream flow. A Pitot tube was used to calibrate the freestream velocity. Raw output from two different sensors driven at two different constant currents are shown in Fig. 15. When the $1/3$ power of the shear stress (converted from the velocity information) is plotted against the voltage, a linear relation is obtained as shown in Fig. 16, which is predicted by Eq. (5).

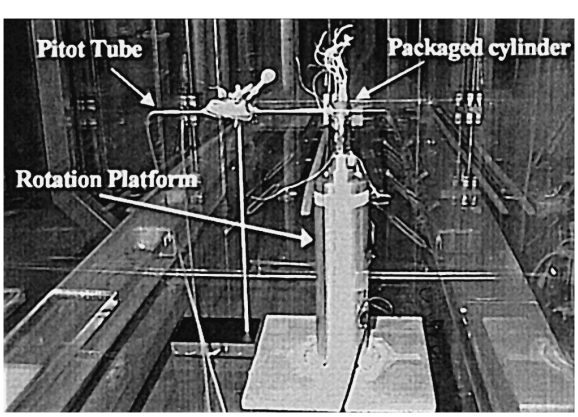

Fig. 14. Windtunnel setup for the shear stress measurement using the sensors on the quartz substrate.

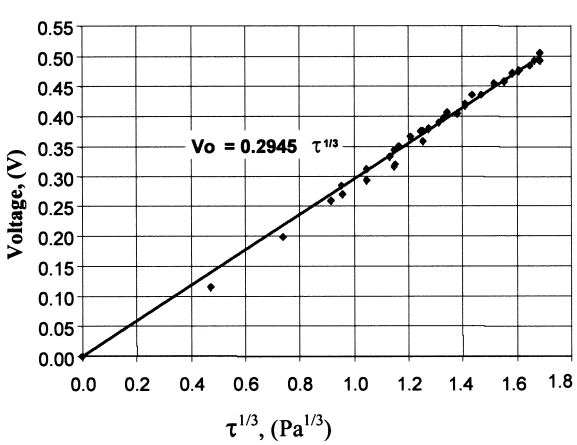

Fig. 16. The voltage output the sensors driven with a constant current source is proportional to the $1/3$ power of the shear stress.

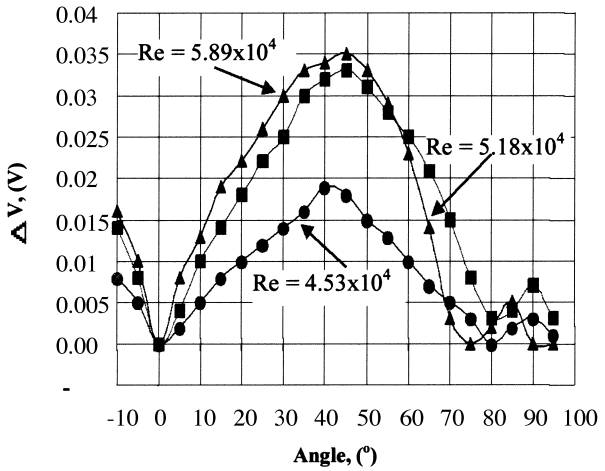

Fig. 17. Raw output of shear stress sensors showing a local minimum at $\theta - 80°$ for various freestream velocities.

5.3. Flow separation

The shear stress on the surface of a body depends on the velocity gradient in the boundary layer. The velocity vectors in the boundary layer are initially parallel and uniform in direction at a local point. However, due to kinetic energy loss through friction or the geometry of the body, an adverse pressure gradient is created in the boundary layer. This adverse pressure gradient will cause local flow reversal in the boundary layer. The location in the boundary layer where this flow reversal initially occurs is defined as the separation point. Mathematically, the velocity gradient is zero, and hence, the shear stress is zero at this point. For a cylinder in a laminar freestream flow, separation usually occurs at $\sim 80°$ circumferentially from the flow stagnation point. As shown in Fig. 17, the shear stress sensors were used to detect the separation point for different flow Reynolds numbers (velocity dependent). The separation point is indicated by the local minimum voltage output in the figure.

6. Conclusion

A novel method was developed to directly fabricate micron-sized structures onto contour surfaces. This method removes the constraint set by the highly developed integrated circuit technology to make micro structures only on planar substrates. Using flexible masks and customized alignment systems, microstructures were built onto 2″ long quartz cylindrical substrates that have diameters of 1.25″. Presently, 5 μm wide structures can be patterned around the surface of quartz cylinders with $\sim 20\%$ yield. The yield increases to $\sim 50\%$ for 10 μm structures, $\sim 70\%$ for 20 μm structures, and $\sim 90\%$ for structures 30 μm and wider.

A dry-release process was developed to sacrificially release metal structures using photoresist as the sacrificial layer. Various microstructures were fabricated on the cylindrical surface and were used as temperature sensors, shear stress sensors, and thermal actuators. The thermal sensors have a TCR of 0.2%/°C. If operated with a constant current source of ~ 50 mA these sensors can be used as shear stress sensors that are able to detect the separation point for flow over a cylinder at Re $\sim 5 \times 10^4$.

We will now proceed to build a system of sensors and actuators to investigate flow control around the cylinder. Suitable thin film materials will be used to optimize the performance of these sensors and actuators.

Acknowledgements

We would like to thank Mr. Edward Fortier III for his remarkable technical skills and invaluable suggestions on building and refining the mechanical systems needed for fabrication. Special thanks also to Dr. Tony Tang and Dr. William C. Tang for the usage of the Micro Devices Laboratory equipment at JPL.

References

[1] C.M. Ho, et al., Control of Macro Machine by Micro Actuators, Bull. of 47th Ann. Meet. of the Div. of Fluid Dyn. of the APS, Atlanta, Nov. 1994.
[2] B. Gupta et al., Analog VLSI system for active drag reduction, IEEE Micro. 16 (5) (1996) 53–59.
[3] S.C. Jacobsen, M. Olivier, Integrated Sensor Network Project, MEMS PI Meet. Rep. Sarcos Res., July 1995–Jan. 1996.
[4] W.F. Dunn, MEMS-Based Smart Tires, 1st Quart. Tech. Report #GDYR1-15-96S, The Goodyear Tire and Rubber, Sept. 1995.
[5] Yablonovitch et al., Extreme selectivity in the lift-off of epitaxial GaAs films, Appl. Phys. Lett. 51 (26) (1987) .
[6] G.J. Sullivan et al., Electron. Lett. 29 (1993) 1890.
[7] C.M. Ho, Y.C. Tai, D. Miu, Conformable M^3 Microsys. for Aerodyn. Control, Semi-Ann. Rep. for ARPA, UCLA/CIT, Jan.–July 1995.
[8] S.C. Jacobsen, et al., Fabrication of Micro-Structures Using Non-Planar Lithography, MEMS91', pp. 63–67.
[9] R.J. Jackman et al., Fabrication of submicrometer features on curved substrates by microcontact printing, Science 269 (4) (1995) 665–665.
[10] K. Takahata, et al., Fine Surface Finishing Method for 3-Dimensional Micro Structures, MEMS96', pp. 73–78.
[11] W.J. Li, C.M. Ho, MEMS on Bulk Contour Mechanical Substrates, Transducers 97', Chicago, 1997.
[12] W.M. Moreau, Semiconductor Lithography, Principles, Practices, and Materials, Plenum, NY, 1988.
[13] W.B. Glendinning, J.N. Helbert, Handbook of VLSI Microlithography, Principles, Technology, and Application, Noyes Publications, NJ, 1991.
[14] W.J. Li, PhD Dissertation: MEMS on Contoured Substrates, Nov. 1997, UCLA.

Wen J. Li received the BS and MS degrees in Aerospace Engineering from the USC in 1987 and 1989, respectively. His industrial experiences include The Aerospace Corporation (1987 to 1995), Silicon Micro-structures (summer of 1994), and the Jet Propulsion Laboratory (1995 to 1997). He began his PhD studies at UCLA in 1992, and received his PhD degree in 1997 specializing in MEMS. Dr. Li joined the faculty of the Department of Mechanical and Automation Engineering of the Chinese University of Hong Kong in 1997. His current research interest is to develop decision making mechanical structures for biomedical, robotic, and automotive applications.

John D. Mai is currently a doctoral candidate in MEMS in the Mechanical and Aerospace Engineering Department at UCLA. He is currently developing a MEMS impinging jet heat exchanger for micro electronic cooling as a joint project between UCLA's Center for Micro Systems and Caltech. He also holds BS And MS degrees in Aerospace Engineering from UCLA. His MS thesis involved characterization of a MEMS shear stress sensor in a compressible flow conducted at Wright Laboratories (USAF). He is currently also a member of the In-Situ Devices Group, Jet Propulsion Laboratory, where he is involved in the fabrication of micro seismometers for next millenium interplanetary probes.

Chih-Ming Ho received his PhD in Mechanics from Johns Hopkins University in 1974 and his BS in Mechanical Engineering from National Taiwan University in 1967. He is the Ben Rich Lockheed Martin Endowed Chair of Advanced Aerospace Technologies in the Mechanical and Aerospace Engineering Department, and the Director of the Center for Micro Systems at UCLA. He was a faculty member of Aerospace Engineering at the USC from 1975 to 1991. He is a member of the US National Academy of Engineering, a Fellow of the American Physical Society (APS), and a Fellow of the American Institute of Aeronautics and Astronautics (AIAA). He has contributed in the areas of turbulence, MEMS, aerodynamics, aeroacoustics and bio fluid dynamics. He has published more than one hundred papers and received several US patents in these fields. He has presented numerous keynote talks in national and international conferences. He has served on national and international committees on science and industrial development. He was an Associate Editor of the ASME Journal of Fluids Engineering from 1990 to 1993 and was the Associate Editor of the AIAA Journal from 1985 to 1987.